

# Triple Correlations

ADOLF W. LOHMANN AND BERNHARD WIRNITZER

*Invited Paper*

The (auto)triple correlation  $I^{(3)}(t_1, t_2)$  is defined as the triple function integral, applied to the signal  $I(t)$

$$I^{(3)}(t_1, t_2) = \int I(t) I(t + t_1) I(t + t_2) dt.$$

The triple correlation  $I^{(3)}(t_1, t_2)$  is less popular than the standard (double) correlation  $I^{(2)}(t_1)$  for several reasons:  $I^{(2)}$  is sometimes easier to observe and to process,  $I^{(3)}$  is small for many bipolar or complex signals, the mathematics associated with  $I^{(2)}$  is better known.

On the other hand, the triple correlation  $I^{(3)}$  knows more about the signal  $I$  than does the ordinary autocorrelation  $I^{(2)}$ . Also  $I^{(3)}$  is in some ways more sensitive, in other ways less sensitive to noise, to bias drifts, etc. Hence, there are situations, where it is quite favorable to evaluate one-dimensional signals or two-dimensional pictures by means of their triple correlations.

We will review the underlying mathematical tools and report on our projects where triple correlations were employed for studying laser pulse shapes, sound quality, halftone print statistics, mobility of bacteria, and astronomical speckle interferometry. We will mention also how others have used the triple correlation for ocean waves, engine noises, intensity interferometry, and other optical signal processing tasks.

## I. INTRODUCTION

### A. Definitions

In some of the following projects we deal with temporal signals  $I(t)$  and their spectra  $\tilde{I}(f)$

$$I(t) = \int \tilde{I}(f) \exp(2\pi j f t) df. \quad (1)$$

In our notation the common autocorrelation is written as

$$I^{(2)}(t_1) = \int I(t) I(t + t_1) dt$$

$$\tilde{I}^{(2)}(f_1) = \int I^{(2)}(t_1) \exp(-2\pi j f_1 t_1) dt_1 = \tilde{I}(f_1) \tilde{I}(-f_1). \quad (2)$$

Among higher order correlations we are interested here essentially in the triple correlation  $I^{(3)}(t_1, t_2)$  and its Fourier transform  $\tilde{I}^{(3)}(f_1, f_2)$ , which is called the "bispectrum."

$$I^{(3)}(t_1, t_2) = \int I(t) I(t + t_1) I(t + t_2) dt \quad (3)$$

$$\tilde{I}^{(3)}(f_1, f_2) = \int \int I^{(3)}(t_1, t_2) \exp[-2\pi i(f_1 t_1 + f_2 t_2)] dt_1 dt_2. \quad (4)$$

This definition of the triple correlation and the bispectrum

Manuscript received December 29, 1983.

The authors are with the Physikalisch-Technische Bundesanstalt, D-8520 Erlangen-Nürnberg, Federal Republic of Germany.

is sensible in the case of deterministic and stochastic signals. In the case of stochastic signals some authors replace  $I(t)$  by  $I(t) - \langle I(t) \rangle$ , yielding a somewhat different definition for the bispectrum. An elegant formulation of this definition and various consequences thereof are given, for example, by Sato [30]. In some other projects our signals are pictures, i.e., functions of the two spatial variables  $(x, y)$ . The associated spatial frequency variables are  $(u_x, u_y)$ . For brevity, we write  $x$  and  $u$  as two-dimensional vectors. The product  $u \cdot x$  is the dot product of these two vectors. The triple correlation of a picture signal is four-dimensional  $(x_1, y_1, x_2, y_2)$ . A more detailed list of notation is provided in the following subsection.

### B. Notations

$t$	Time coordinate.
$f$	Temporal frequency.
$x$	Space coordinate (two-dimensional vector).
$u$	Spatial frequency (two-dimensional vector).
$I(t)$	Time signal.
$I^{(2)}(t_1)$ $= \int I(t) I(t + t_1) dt$	Temporal autocorrelation.
$I^{(3)}(t_1, t_2)$ $= \int I(t) I(t + t_1) I(t + t_2) dt$	Temporal triple correlation.
$I_{nmk}^{(3)}(t_1, t_2)$ $= \int I_n(t) I_m(t + t_1) I_k(t + t_2) dt$	Temporal triple cross correlation.
$\tilde{I}(f)$	Temporal frequency spectrum.
$\tilde{I}^{(2)}(f_1)$ $= \tilde{I}(f_1) \tilde{I}(-f_1)$	Fourier transform of $I^{(2)}(t_1)$ .
$\tilde{I}^{(3)}(f_1, f_2)$ $= \tilde{I}(f_1) \tilde{I}(f_2) \tilde{I}(-f_1 - f_2)$	Temporal bispectrum.
$\tilde{I}_{nmk}^{(3)}(f_1, f_2)$ $= \tilde{I}_n(f_1) \tilde{I}_m(f_2) \tilde{I}_k(-f_1 - f_2)$	Temporal cross bispectrum.
$\tilde{I}_x(f)$	Complex spectrogram.
$\tilde{I}_r(f_1, f_2)$	Complex bispectrogram.
$\varphi(f)$	Phase of $\tilde{I}(f)$ .
$\varphi^{(2)}(f_1)$	Phase of $\tilde{I}^{(2)}(f_1)$ .
$\varphi^{(3)}(f_1, f_2)$	Phase of $\tilde{I}^{(3)}(f_1, f_2)$ .
$I(x)$	Spatial signal.
$I^{(2)}(x_1)$	Spatial autocorrelation of $I(x)$ .
$I^{(3)}(x_1, x_2)$	Spatial triple correlation of $I(x)$ .

$\tilde{I}(\mathbf{u})$	Spatial frequency spectrum.
$\tilde{I}^{(2)}(\mathbf{u}_1)$	Fourier transform of $I^{(2)}(\mathbf{x}_1)$ .
$\tilde{I}^{(3)}(\mathbf{u}_1, \mathbf{u}_2)$	Spatial bispectrum.
$W$	Pulsewidth.
$H^{(1)}(W)$	First-order histogram of the pulsewidth $W$ .
$H^{(2)}(W_A, W_B)$	Second-order histogram.
$H^{(3)}(W_A, W_B, W_C)$	Third-order histogram.

### C. Why Signal Processing with Correlations?

To understand our motivation to study triple correlations it is worthwhile to recapitulate briefly some of the reasons for using the ordinary double correlation. Sometimes, the original signal is not observable, but its autocorrelation is. For example, the complex wave amplitude  $I(\mathbf{x})$  cannot be recorded since optical frequencies ( $10^{15}$  Hz) are too high. However, it is easy to perform a Fourier transform optically, and then to observe the modulus square thereof

$$|\tilde{I}(\mathbf{u}_1)|^2 = \int \left[ \int I(\mathbf{x} + \mathbf{x}_1) I^*(\mathbf{x}) d\mathbf{x} \right] \exp(-2\pi j \mathbf{x}_1 \cdot \mathbf{u}_1) d\mathbf{x}_1. \quad (5)$$

Another example of the usefulness of a double correlation is astronomical speckle interferometry (details in Section V). The signal is the intensity distribution in the output plane of the telescope. This signal fluctuates heavily due to the turbulent atmosphere. The long-time average of the signal spectrum  $\langle \tilde{I}(\mathbf{u}) \rangle$  contains only low frequencies, while the average power spectrum  $\langle |\tilde{I}(\mathbf{u}_1)|^2 \rangle = \langle \tilde{I}^{(2)}(\mathbf{u}_1) \rangle$  has a bandwidth up to the fundamental diffraction limit of the primary mirror.

It must be admitted that the autocorrelation  $I^{(2)}(t_1)$  does not know everything about the signal  $I(t)$  itself. Sometimes, this lack of information is an advantage, if the missing parts are irrelevant.

### D. Why the Third-Order Correlation?

Several arguments are in favor of the second-order correlation  $I^{(2)}(t_1)$ , as compared to the third-order, or triple correlation  $I^{(3)}(t_1, t_2)$ . For example, it takes more computing time and more storage to handle  $I^{(3)}$ .

Someone might suspect that the ensemble average  $\langle I^{(3)} \rangle$  is almost always zero. This suspicion might be based on a theorem known as the Reed or Wang-Uhlenbeck theorem. According to that theorem, all odd-order correlations are zero in average, if the stochastic process  $I(t)$  is Gaussian, stationary, and zero-mean.

The property "Gaussian" is so popular that one might be tempted to believe all signals are Gaussian. Nonetheless, the triple correlation has a right to exist. As we will see in some of the applications in Sections III–VI, the triple correlation is sometimes preferable over the double correlation, since it is possible to deduce almost uniquely the signal  $I(t)$  from  $I^{(3)}$ . The retrieval of  $I(t)$  is seldom possible if only  $I^{(2)}$  is known. Yet another advantage of  $I^{(3)}$  is its lower sensitivity to noise under certain circumstances (see Section II-D).

### E. Our Plan

In Section II we will present the mathematical tools for dealing with the triple correlation. The degree of rigor is application-oriented. Next, in Section III, we report two of our projects, where the signal is one-dimensional in time. The signals describe a laser pulse and a musical tone. In the following section (IV) we apply triple-correlation analysis to pictures: halftone prints and microscopic images of bacteria. Section V is devoted to astronomical speckle interferometry, where triple-correlation analysis enabled us to obtain images that are thirty times sharper than what was standard a few years ago. In the concluding Section VI we will summarize what others have accomplished with the help of triple correlations. Some of those other authors were active in this field before us. We postponed the description of their work to the last chapter for tutorial reasons.

## II. MATHEMATICAL BACKGROUND

### A. Basic Properties of Triple Correlation

One of the earliest references on triple correlations are due to Brillinger [1], as far as we know. There exists apparently no account of the mathematical tools surrounding the triple correlation. This Section is intended to fill the gap. The auto triple correlation has been defined in (3)

$$I^{(3)}(t_1, t_2) = \int I(t) I(t + t_1) I(t + t_2) dt. \quad (3)$$

The Fourier transform thereof, the so-called bispectrum, is related to the signal spectrum  $\tilde{I}(f)$  by

$$\tilde{I}^{(3)}(f_1, f_2) = \tilde{I}(f_1) \tilde{I}(f_2) \tilde{I}(-f_1 - f_2). \quad (6)$$

The bispectrum is 3/4 redundant due to two inherent symmetries

$$\tilde{I}^{(3)}(f_1, f_2) = \tilde{I}^{(3)}(f_2, f_1) = \tilde{I}^{(3)}(-f_1 - f_2, f_1). \quad (7)$$

If the signal  $I(t)$  is real, both the signal spectrum and the bispectrum are Hermitian

$$\tilde{I}(f) = \tilde{I}^*(-f)$$

$$\tilde{I}^{(3)}(f_1, f_2) = \tilde{I}^{(3)}(-f_1, -f_2)^*. \quad (8)$$

In that case, only one angular octant of the  $(f_1, f_2)$  domain of  $\tilde{I}^{(3)}$  is nonredundant.

In addition to the auto triple correlation we may also combine three different signals  $I_K(t)$ ,  $I_L(t)$ , and  $I_M(t)$  into a cross triple correlation

$$I_{K,L,M}^{(3)}(t_1, t_2) = \int I_K(t) I_L(t + t_1) I_M(t + t_2) dt. \quad (9)$$

The cross triple correlation can be obtained by adding nine suitable auto triple correlations. This action might be justified if the multiplication of the three signals causes practical difficulties. The underlying algorithm, called "polarization identity of the third order" [2], is a generalization of the simple rule that allows one to replace multiplication by adding and squaring

$$(a + b)^2 - (a - b)^2 = 4ab. \quad (10)$$

The third-order generalization of (10) utilizes the third root of unity  $W = \exp 2\pi j/3$  and cubic terms

$$\sum_{m,n=0}^2 W^{-(m+n)}(a + W^m b + W^n c)^3 = 6abc. \quad (11)$$

### B. Some Examples

To get a feeling for triple correlations and for the associated bispectra we present here graphic examples for the following signals:

$$I(t) = \text{rect}(t/\Delta t) \quad (\text{see Fig. 1}) \quad (12)$$

$$I(t) = 1 + \cos(2\pi ft) \quad (\text{see Fig. 2}) \quad (13)$$

$$I(t) = A\delta(t - t_0) + B\delta(t + t_0) \quad (\text{see Fig. 3}) \quad (14)$$

$$I(t) = \text{sawtooth periodicity} \quad (\text{see Fig. 4}). \quad (15)$$

### C. Linear Systems Theory

If a system acts in linear and time-invariant fashion upon the signal  $I(t)$ , then this system is also linear and time-invariant for the triple correlation.

To show this we write down the essential equations for the signals  $I_i(t)$  (in-going) and  $I_o(t)$  (out-going), as well as for the impulse response  $P(t)$

$$I_o(t) = I_i(t) * P(t) \quad (16)$$

$$\tilde{I}_o(f) = \tilde{I}_i(f) \cdot \tilde{P}(f). \quad (17)$$

The asterisk  $*$  in (16) represents a convolution.

From (17) and from the definition of the bispectrum (see (6)) it follows immediately that

$$\tilde{I}_o^{(3)}(f_1, f_2) = \tilde{I}_i^{(3)}(f_1, f_2) \cdot \tilde{P}^{(3)}(f_1, f_2). \quad (18)$$

Multiplication in the Fourier domain corresponds to a convolution in the time domain

$$I_o^{(3)}(t_1, t_2) = I_i^{(3)}(t_1, t_2) * P^{(3)}(t_1, t_2). \quad (19)$$

One particular aspect of this linear systems theory refers to low-pass signals. Let us assume the signal spectrum  $\tilde{I}(f)$  remains unchanged if multiplied by the square box  $\text{rect}(f/\Delta f)$

$$\begin{aligned} \tilde{I}(f) &\rightarrow \tilde{I}(f) \text{rect}(f/\Delta f) \\ \text{rect}(f) &= \tilde{P}(f). \end{aligned} \quad (20)$$

Then the same must be true for the associated bispectra

$$\tilde{I}^{(3)}(f_1, f_2) \rightarrow \tilde{I}^{(3)}(f_1, f_2) \cdot \tilde{P}^{(3)}(f_1, f_2). \quad (21)$$

This particular bispectral filter function  $\tilde{P}^{(3)}$  is binary in amplitude, with hexagonal support area in the  $(f_1, f_2)$  domain, as shown in Fig. 5.

As is well-known, if the support in the Fourier domain is finite, the signal may be sampled in the time domain. This, of course, also holds for the two-dimensional Fourier pair of domains  $(t_1, t_2)$  and  $(f_1, f_2)$ . Fig. 5 is helpful for specifying the sampling rate not only for band-limited signals. Due to the symmetrical nature of the Fourier transformation, we may use Fig. 5 also for setting the proper sampling rate for  $\tilde{I}^{(3)}(f_1, f_2)$  if the duration  $\Delta t$  of the signal  $I(t)$  is finite.

### D. The Influences of Bias, Noise, and Nonlinearities

We begin by studying the influence of a bias on a simple signal. The triple correlation is blind to some signals, such

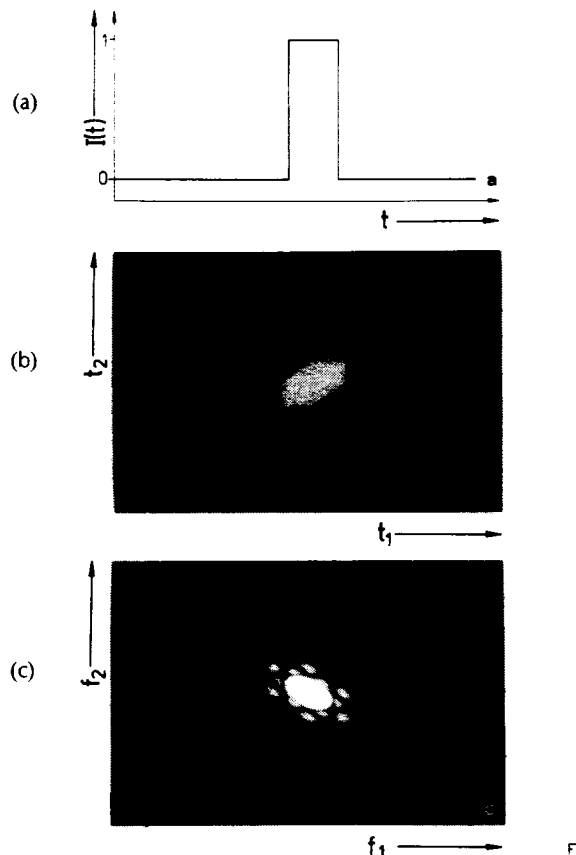


Fig. 1. Triple correlation (b) and bispectrum (c) for a square-box signal (a).

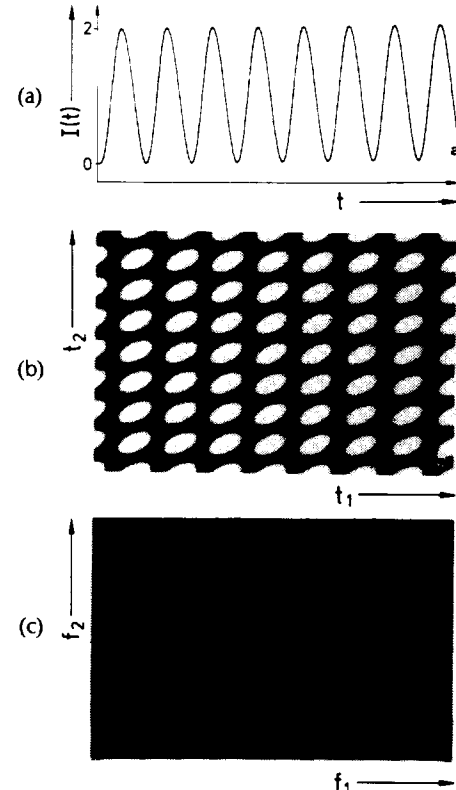


Fig. 2. Triple correlation (b) and bispectrum (c) for a cosine signal on a bias (a).

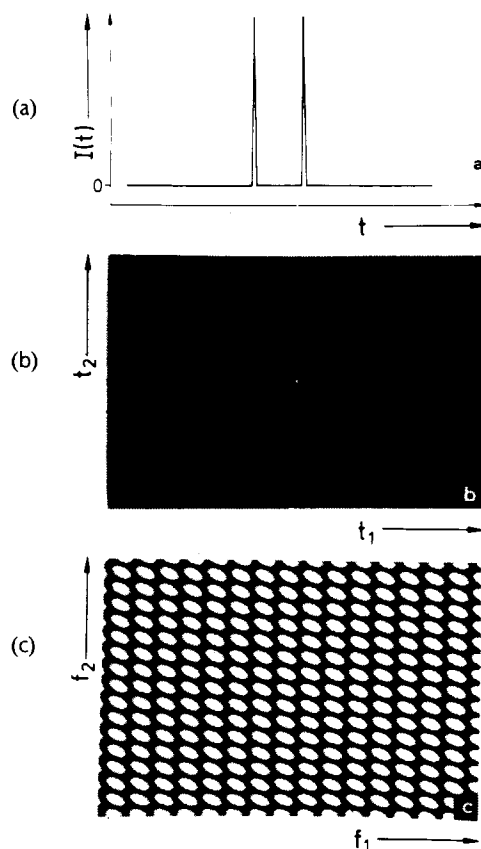


Fig. 3. Triple correlation (b) and bispectrum (c) for a signal, consisting of two spikes (a).

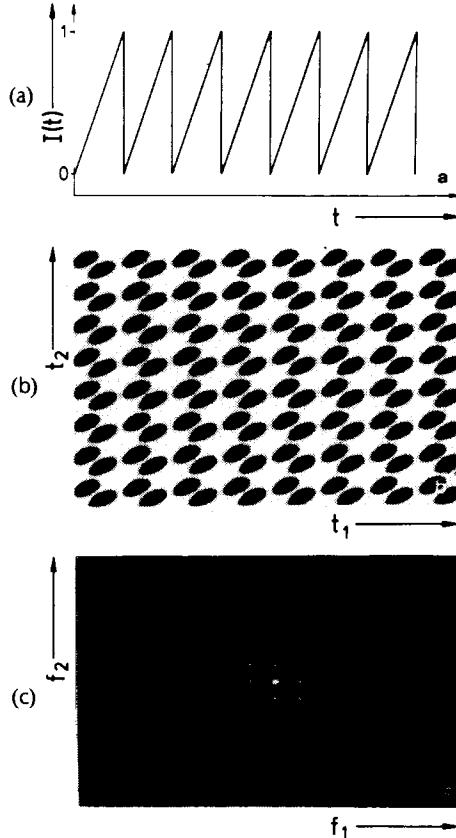


Fig. 4. Triple correlation (b) and bispectrum (c) for a sawtooth-periodical signal (a).

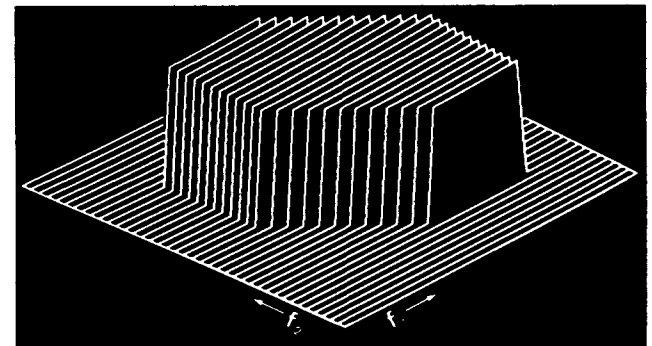


Fig. 5. The bispectral low pass, associated with the square-box low-pass filter function.

as, for example,  $I(t) = \cos(2\pi f_0 t)$ . To see this we enter the other Fourier domain where we have  $2\tilde{I}(f) = \delta(f - f_0) + \delta(f + f_0)$ . Now we plot the bispectrum  $\tilde{I}^{(3)}(f_1, f_2) = \tilde{I}(f_1)\tilde{I}(f_2)\tilde{I}(-f_1 - f_2)$  in the  $(f_1, f_2)$  domain (Fig. 6(a)). Each of the three factors consists of a pair of parallel delta lines. There is no point with three lines in common. Hence,  $\tilde{I}^{(3)}$  is identically zero.

Now we add a bias to the signal  $I(t)$ , or equivalently a delta line  $\delta(f)$  to the signal spectrum  $\tilde{I}(f)$ . In  $\tilde{I}^{(3)}$  this new delta line appears three times, two times on the  $f_1$ - and  $f_2$ -axis, and furthermore, as the third dotted line in Fig. 6(b). Now there are 7 points where the bispectrum is nonzero.

We learned from this example that a triple-correlation measurement might be a very sensitive test for detecting the presence of a bias.

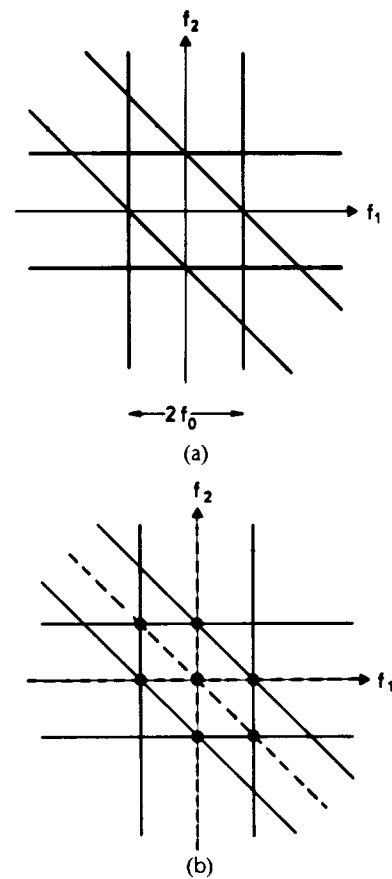


Fig. 6. Graphic construction of the bispectrum for a pure-cosine signal  $\cos(2\pi f_0 t)$  without bias (a), and with bias (b).

Similarly, we might use the triple correlation for detecting weak nonlinearities of an apparatus. Suppose we feed the apparatus with a pure cosine signal  $\cos(2\pi f_0 t)$ , without bias. The associated triple correlation is zero. But if the apparatus responds not only with the base frequency but also with the second-harmonic  $\cos(4\pi f_0 t)$ , then the triple correlation will be nonzero. This can be understood easily by means of a graphic construction of the bispectrum for the distorted harmonic signal, similar to that in Fig. 6.

Now let us consider the influence of noise upon the triple correlation. The case of photon noise, or shot noise, is important when astronomers observe very faint objects. The triple correlation reacts favorably in the presence of photon noise, as will be shown in detail in Section V-C.

If the detector is responsible for the noise, the following assumptions are sensible: the noise is signal-independent additive and stationary. This model is described by the two following equations:

$$I(t) + N(t) = J(t) \quad (22)$$

$$\begin{aligned} \langle J^{(3)}(t_1, t_2) \rangle &= I^{(3)}(t_1, t_2) + \langle N^{(3)}(t_1, t_2) \rangle \\ &+ \langle N \rangle [I^{(2)}(t_1) + I^{(2)}(t_2) \\ &+ I^{(2)}(t_2 - t_1)] \\ &+ \int I(t) dt \cdot [\langle N^{(2)}(t_1) \rangle \\ &+ \langle N^{(2)}(t_2) \rangle + \langle N^{(2)}(t_2 - t_1) \rangle]. \end{aligned} \quad (23)$$

Under favorable conditions all of the noise-related terms may vanish. If the mean of the noise  $\langle N \rangle$  is zero, the second-order correlation  $I^{(2)}$  of the signal cannot contribute to the overall triple correlation  $\langle J^{(3)} \rangle$ . If the signal  $I(t)$  itself is zero in average, the autocorrelation of the noise  $\langle N^{(2)} \rangle$  loses its impact. The remaining term  $\langle N^{(3)} \rangle$  might be negligible if the probability density function  $p(N)$  is symmetrical,  $p(N) = p(-N)$ , or at least not skewed:  $\int N^3 p(N) dN = 0$ . By adding (or subtracting) a suitable bias from  $J(t)$  it is always possible to eliminate at least one of the three noise-related terms in (23).

#### E. Limitations of Signal Retrieval from the Triple Correlation

Before going into details of signal retrieval from triple correlations, we present some fundamental limitations. These limitations become obvious by considering invariance properties of the Fourier transform of the triple correlation, the bispectrum.

Using the definition of the bispectrum (6) we find that the bispectrum is immune to a factor  $\exp(\beta f)$  in the spectrum, i.e., for

$$\tilde{I}_F(f) = \tilde{I}(f) \exp(\beta f), \quad \beta: \text{complex constant}$$

we find

$$\begin{aligned} \tilde{I}_F^{(3)}(f_1, f_2) &= \tilde{I}(f_1) \cdot \tilde{I}(f_2) \cdot \tilde{I}(-f_1 - f_2) \\ &\cdot \exp(\beta[f_1 + f_2 - f_1 - f_2]) \\ &= \tilde{I}^{(3)}(f_1, f_2). \end{aligned} \quad (24)$$

Many counter-examples for a unique signal reconstruction from the bispectrum or the triple correlation can be traced back to (24). The counter-example given by Grünbaum [3] is similar in nature. Equation (24) also includes the special case when a linear phase factor in the spectrum will

not influence the bispectrum, or equivalently, the triple correlation cannot distinguish between  $I(t)$  and  $I(t - t_0)$ .

Another class of signals which cannot be reconstructed from their triple correlation are those of skewness zero or, in other words, those whose triple correlation is zero, as already discussed in the previous section.

#### F. Retrieval of a Signal from its Triple Correlation

"If  $I(t)$  is real and of finite extent, then it is possible to retrieve  $I(t)$  (apart from a shift) from  $I^{(3)}(t_1, t_2)$ ."

We shall sketch the proof of this statement and we shall generalize it to complex  $I(t)$ . We first present a plausibility proof in a graphic format. In the two-dimensional domain  $(t_1, t_2)$  of  $I^{(3)}(t_1, t_2)$  we concentrate on the edge in the  $t_1$  direction. There, the first two factors within the  $I^{(3)}$  integral barely overlap, as shown in Fig. 7. Hence, these factors

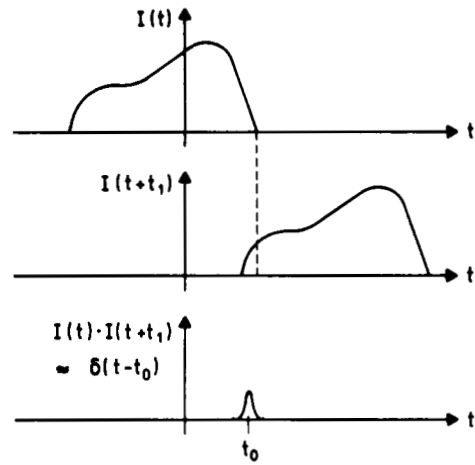


Fig. 7. For the retrieval proof:  $I(t + t_1)$  is shifted so far that its product with  $I(t)$  is like a delta function.

together form in essence a delta. As a consequence, the triple correlation is almost like the signal itself

$$I^{(3)}(t_1, t_2) \approx \int \delta(t - t_0) I(t + t_2) dt = I(t_0 + t_2). \quad (25)$$

For more details see [4].

A more rigorous proof of our claim that a signal can be reconstructed from its triple correlation almost uniquely, can be given in terms of analytic functions. The proof is performed in the Fourier domain and is sketched now.

For an  $I(t)$  of finite extent,  $\tilde{I}(f)$  can be continued analytically by extending  $f$  to a complex variable  $z = z' + jz''$ . The analytic continuation  $\tilde{I}(z)$  is determined by its complex zeros  $z_n$ , and can be written as a Hadamard product

$$\tilde{I}(z) = \exp(\alpha + \beta z) \prod_n (z - z_n) \exp(z/z_n). \quad (26)$$

This fundamental equation of the theory of complex functions cannot be extended to any arbitrary function of two variables. However, in our situation, we know how the two-dimensional  $\tilde{I}^{(3)}(z_1, z_2)$  is related to the one-dimensional  $\tilde{I}(z)$

$$\tilde{I}^{(3)}(z_1, z_2) = \tilde{I}(z_1) \tilde{I}(z_2) \tilde{I}(-z_1 - z_2). \quad (27)$$

Hence, we may insert (26) into (27)

$$\tilde{I}^{(3)}(z_1, z_2) = \exp(3\alpha) \prod_n (z_1 - z_n)(z_2 - z_n) \cdot (-z_1 - z_2 - z_n). \quad (28)$$

Based on this equation we may derive from the complex zero subspaces of  $\tilde{I}^{(3)}(z_1, z_2) = 0$  the particular complex zeros of  $\tilde{I}(z)$ . Once we know the  $z_n$ , we can compute  $I(z)$ , hence  $\tilde{I}(f)$ , and hence  $I(t)$ . The detailed presentation of this proof [5] shows that for the general case of complex  $I(t)$ ,  $\tilde{I}(f)$  can be reconstructed up to an exponential factor  $\exp[\alpha + \beta f]$ , with  $\beta$  a complex constant and  $\alpha = 0, 2\pi j \cdot 1/3$  or  $2\pi j \cdot 2/3$ .

### G. A Retrieval Algorithm

The details of this algorithm and a successful utilization thereof for astronomical purposes is presented elsewhere [4], [5]. Here, we shall sketch only the philosophy of this algorithm, which is performed in the frequency domain.

For the sake of simplicity we assume reality of the signal  $I(t)$  and hence Hermitian symmetry of the spectrum  $\tilde{I}(-f) = I^*(f)$ . We begin by setting  $f_2 = 0$  in  $\tilde{I}^{(3)}(f_1, f_2)$

$$\tilde{I}^{(3)}(f_1, 0) = \tilde{I}(f_1)\tilde{I}(0)\tilde{I}(-f_1) = |\tilde{I}(f_1)|^2\tilde{I}(0). \quad (29)$$

Hence, the Fourier amplitude  $|\tilde{I}(f)|$  is available directly on the  $f_1$ -axis of  $\tilde{I}^{(3)}$ .

Now we want to retrieve the Fourier phase  $\varphi(f)$ , defined by  $\tilde{I} = |\tilde{I}| \exp(j\varphi)$ . To that end we concentrate on a straight line, parallel to the  $f_1$ -axis, but above it by one sampling step  $\delta f$

$$\begin{aligned} \tilde{I}^{(3)}(f_1, \delta f) &= \tilde{I}(f_1)\tilde{I}(\delta f)\tilde{I}(-f_1 - \delta f) \\ &= \tilde{I}(\delta f) \cdot |\tilde{I}(f_1) \cdot \tilde{I}(-f_1 - \delta f)| \\ &\quad \cdot \exp[j\varphi(f_1) - j\varphi(f_1 + \delta f)]. \end{aligned} \quad (30)$$

Defining  $\varphi^{(3)}(f_1, f_2)$  as phase of  $\tilde{I}^{(3)}$ , we can extract from (30) the following phase equation:

$$\varphi^{(3)}(f_1, \delta f) = \varphi(\delta f) + [\varphi(f_1) - \varphi(f_1 + \delta f)]. \quad (31)$$

From here we can extract  $\varphi(f_1)$  itself, apart from an additive constant, and a term linear in  $f_1$ , that reflects the lack of knowledge about the  $t_0$  in  $I(t - t_0)$ .

Finally, we note that in the complete algorithm the variable  $\delta f$  in (31) is scanned over a wide range in order to bolster the signal-to-noise ratio (SNR) of the reconstructed phases  $\varphi(f_1)$ .

### H. Comparison with other Correlations

The Fourier transform of the second-order correlation is

$$\tilde{I}^{(2)}(f_1) = \tilde{I}(f_1)\tilde{I}(-f_1). \quad (32)$$

The associated phase equation is

$$\varphi^{(2)}(f_1) = \varphi(f_1) + \varphi(-f_1). \quad (33)$$

Hence, the second-order correlation contains only the symmetric part of the Fourier phase  $\varphi(f_1)$ . This symmetric phase is zero if  $I(t)$  is real. Hence, it might be said, that the second-order correlation is "phase-blind." The fourth-order correlation behaves similarly.

But the sixth-order correlation is interesting again, especially if every second factor under the integral is conjugated

and if  $t_1 = 0$ ,  $t_3 = t_2$ , and  $t_5 = t_4$

$$\begin{aligned} I^{(6)}(t_1 = 0, t_2, t_2, t_4, t_4) \\ = \int |I(t)|^2 \cdot |I(t + t_2)|^2 \cdot |I(t + t_4)|^2 dt. \end{aligned} \quad (34)$$

Equation (26) can also be interpreted as the third-order correlation of a positive signal.

If  $I(t)$  is a zero-mean stationary Gaussian random process, we obtain as the average correlation

$$\begin{aligned} \langle |I(t)|^2 |I(t + t_1)|^2 |I(t + t_2)|^2 \rangle &= J^{(2)}(0)^3 + J^{(2)}(0) \\ &\quad \cdot [J^{(2)}(t_1)^2 + J^{(2)}(t_2)^2 + J^{(2)}(t_2 - t_1)^2] \\ &\quad + 2 \operatorname{Re} [J^{(2)}(t_1) \cdot J^{(2)}(-t_2) \cdot J^{(2)}(t_2 - t_1)] \end{aligned} \quad (34')$$

with the abbreviation  $J^{(2)}(t_1) = \langle I(t)I^*(t + t_1) \rangle$ . This equation, which is due to Gamo, is valuable because the last term ( $2 \operatorname{Re} \dots$ ) knows something about the phase of  $J^{(2)}$ . By contrast, the corresponding fourth-order correlation  $\langle |I(t)|^2 |I(t + t_1)|^2 \rangle$  is completely phase-blind as far as  $J^{(2)}$  is concerned.

Gamo [6], [7] proposed to use the triple correlation in (34) and (34') for astronomical and spectroscopic purposes. This correlation integral will also reappear shortly in Section III-A.

## III. SOME PROJECTS WITH ONE-DIMENSIONAL SIGNALS

### A. Measurement of Ultrashort Laser Pulses

Some years ago it became possible to produce laser pulses much shorter than a picosecond. Since that time, a new field of research has developed in order to study physical phenomena on a femtosecond time scale. Meanwhile, the pulse durations reported by experimentalists are approaching the theoretical limitations. At the moment the world record is held by a pulse of 30-fs duration.

No detector is fast enough to measure such ultrashort pulses directly. However, there exist various methods for measuring the autocorrelation function of the pulse intensity [8]. Unfortunately, the autocorrelation is symmetrical and therefore any asymmetry of the underlying pulse is hidden.

At this point we can benefit from an  $I^{(3)}$  analysis which can provide the true pulse shape instead of the autocorrelation, as suggested in [9] and discussed now.

In Fig. 8, a triple-intensity interferometer is shown which can be used to record the raw data of the experiment. For a sequence of pulses, the three legs of the interferometer provide mutually delayed pulse trains with amplitudes  $I(t)$ ,  $I(t + t_1)$ , and  $I(t + t_2)$ . Mixing of these pulse trains in a nonlinear crystal yields, by the way of third-harmonic generation, the intensity triple correlation

$$I^{(3)}(t_1, t_2) = \int |I(t)|^2 |I(t + t_1)|^2 |I(t + t_2)|^2 dt. \quad (35)$$

Once the intensity triple correlation of the pulse is known, also the pulse shape  $|I(t)|^2$  can be reconstructed as discussed in Section II-G. In a simulation experiment (Fig. 9) it is illustrated that the reconstruction is very insensitive to noise in the raw data. The noise is assumed to be signal-independent, white additive, and stationary.

$$|\tilde{I}(f)|^2 = \tilde{I}(f)\tilde{I}(f)^*. \quad (36)$$

For a musical tone, for example, the power spectrum shows how the fundamental frequency and its higher harmonics compose to form the timbre of the tone (see Fig. 10). However, the power spectrum, being "phase-blind,"

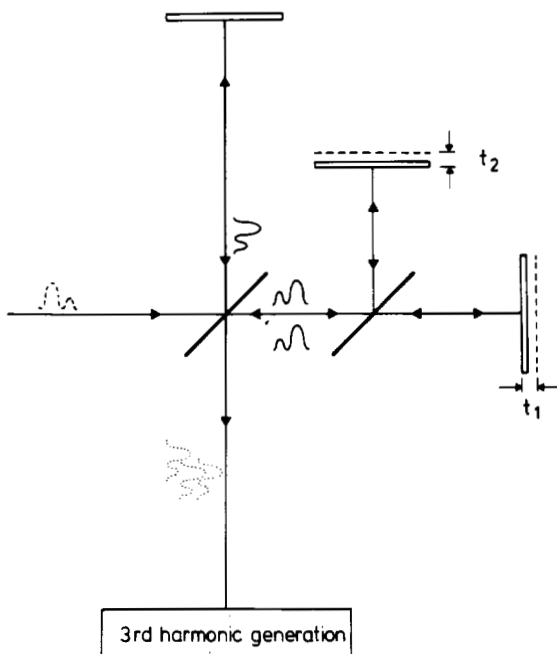


**Fig. 8.** A triple-intensity interferometer can be used to record the intensity triple correlation of a pulse train.

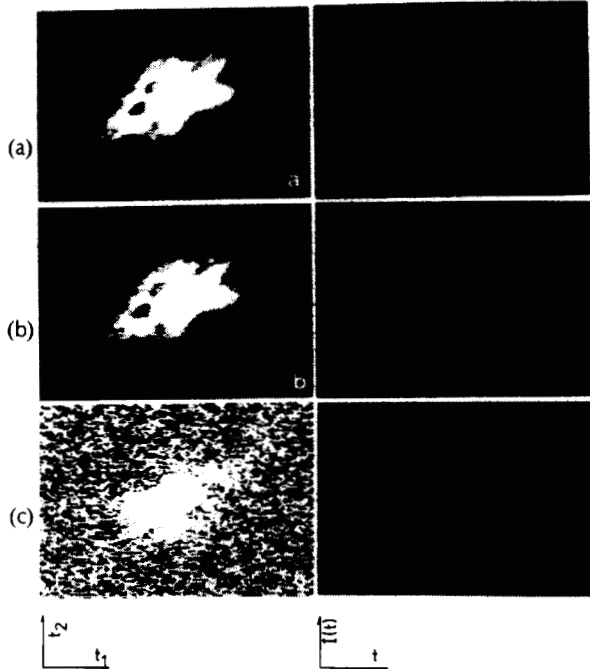
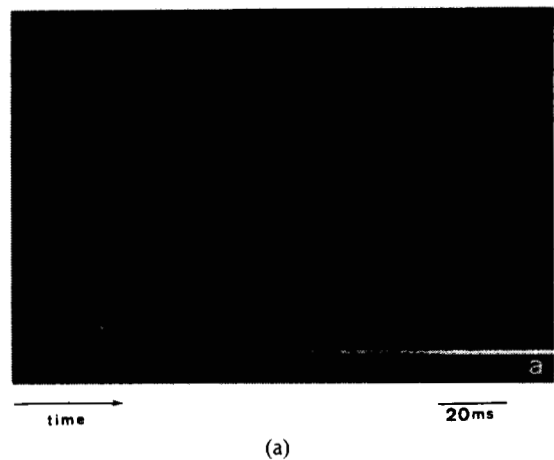


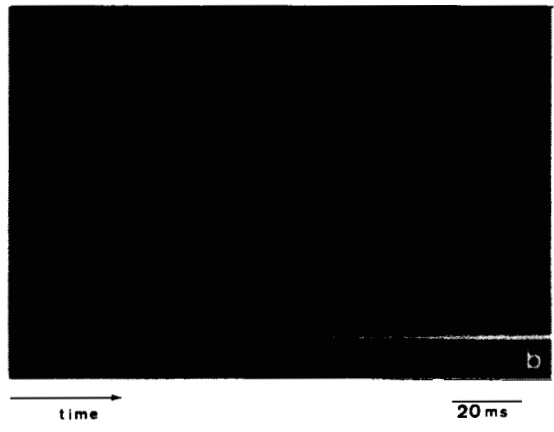
**Fig. 9.** Signal reconstruction from triple correlations. From the intensity triple correlation of the pulse shape (left column), the true pulse shape can be reconstructed (right column). The SNR in the triple correlation was (a) 4, (b) 2, (c) 0.4. The higher SNR of the reconstructed pulse shapes is due to redundant signal information which is contained in the triple correlation (for further details see [9]).

#### B. Higher Order Spectrograms of Musical Tones

The human voice or a musical tone can be described as air pressure  $I(t)$  as a function of time. It is sensible to express the same signal in the Fourier domain by its power spectrum



(a)



(b)

**Fig. 10.** Musical timbre, presented as a spectrogram. Tone "a" of a flute of good quality (a) and of a flute of poor quality (b).

cannot reveal the relative phases between the harmonic components. This phase blindness may not bother us too much, since the human ear is almost deaf to the phase differences as well. However, the ear can perceive time-varying phase differences between different frequency components of a tone.

In order to study such effects we extended the concept of spectrograms to higher order correlations. The complex spectrogram is a description in frequency and time obtained by computing the Fourier transform of the signal multiplied by a window function  $W(t)$

$$\tilde{I}_r(f) = \int I(t)W(t-\tau) \exp[-2\pi jft] dt. \quad (37)$$

The modulus square of  $\tilde{I}_r(f)$  is called the spectrogram of  $I(t)$  (Fig. 10). By extending the definition of the bispectrum (see (6)) we define the complex bispectrogram as

$$\tilde{I}_r^{(3)}(f_1, f_2) = \tilde{I}_r(f_1)\tilde{I}_r(f_2)\tilde{I}_r(-f_1 - f_2). \quad (38)$$

A generalization to spectrograms of the  $n$ th order is straightforward. The bispectrum reveals the mutual amplitude and phase relation between the frequency compo-

nents  $f_1, f_2$  and  $(-f_1 - f_2)$ . For  $f_1 = f_2$  we obtain

$$\begin{aligned} |\tilde{I}_r^{(3)}(f_1, f_1)| &= |\tilde{I}_r(f_1)|^2 |\tilde{I}_r(2f_1)| \\ \varphi_r^{(3)}(f_1, f_1) &= 2\varphi_r(f_1) - \varphi_r(2f_1) \end{aligned} \quad (39)$$

as exploited in the experiment in Fig. 11.

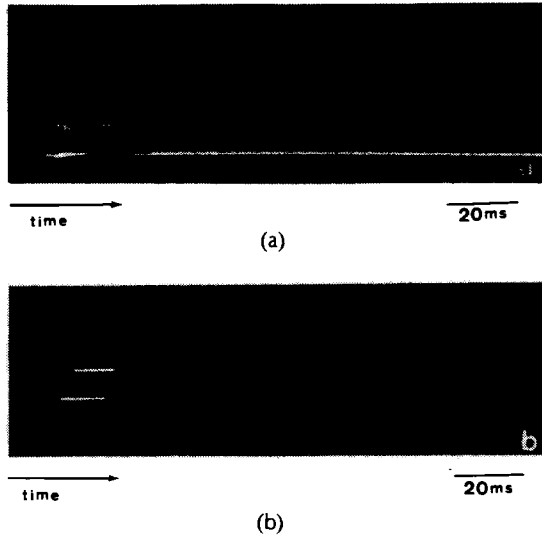


Fig. 11. Phase of the complex bispectrum. Tone "a" of a flute of good quality (a) and of a flute of poor quality (b). The phase values ( $-\pi$  to  $+\pi$ ) are displayed as intensities.

#### IV. SOME PROJECTS WITH TWO-DIMENSIONAL SIGNALS

##### A. Conditional Histograms in Halftone Pictures

The fine structure of a halftone image is binary (black or white). Grey values are implemented by spatial pulsewidth modulation, properly generalized to two dimensions ( $x, y$ ). For the sake of brevity we shall stick to one dimension ( $x$ ) in this section and in the associated Fig. 12. Our goal is to determine histograms of the pulsewidths  $W$ . The first-order

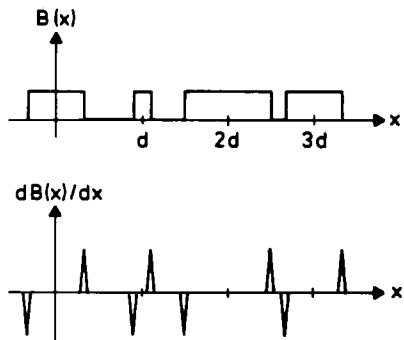


Fig. 12. A halftone image and its derivative.

histogram  $h^{(1)}(W)$  describes the frequency of occurrence of the grey values that are implemented by the associated pulsewidths  $W$ . The second-order histogram  $h^{(2)}(W_A, W_B)$  is proportional to the joint probability of finding the width  $W_A$  at  $x = md$  and the width  $W_B$  adjacent to it, at  $x = (m + 1)d$ . The third-order histogram  $h^{(3)}(W_A, W_B, W_C)$  describes the coupling of three adjacent pixels. This  $h^{(3)}$  has some-

thing to do with the triple correlation, as we shall see shortly.

Histograms of pictures, or of whole sets of pictures, are needed for computing the average information content per pixel. The problem of computing this entropy measure is quite similar to computing the entropy of a single word of a typical text in English, for example.

Histograms of halftone pictures can be measured by means of an optical correlation experiment [10]. The first step of the experiment consists of forming the derivative  $dB(x)/dx$  (Fig. 12). Every pulse is converted into a pair of spikes with opposite polarity. Then this derivative  $dB(x)/dx$  is correlated with a spike pair of width  $W$ . The result is squared, which occurs automatically in coherent optical filtering. The output values from locations  $x = md$  are added to yield the first-order histogram, apart from a constant factor. The associated equations are

$$\begin{aligned} B(x) &= \sum_{m=1}^M \text{rect}\left(\frac{x - md}{W_m}\right) \\ \frac{dB(x)}{dx} \otimes \frac{d}{dx} \left\{ \text{rect}\left(\frac{x}{W}\right) \right\} &= B^{(1)}(x; W) \\ \sum_m |B^{(1)}(md; W)|^2 &= \text{const} \cdot h^{(1)}(W). \end{aligned} \quad (40)$$

For determining the second-order histogram  $h^{(2)}(W_A, W_B)$  the experiment is similar. However, the double pulse signal  $d/dx\{\text{rect}(x/W)\}$  is now replaced by two adjacent double pulses of widths  $W_A$  and  $W_B$

$$\frac{d}{dx} \left\{ \text{rect}\left(\frac{x}{W_A}\right) + \text{rect}\left(\frac{x - d}{W_A}\right) \right\}. \quad (41)$$

From the final result  $|B^{(2)}(md; W_A, W_B)|^2$  we have to subtract single-coincidence contributions  $h^{(1)}(W_A)$  and  $h^{(1)}(W_B)$ , before obtaining the joint histogram  $h^{(2)}(W_A, W_B)$ . Empirically we found that  $h^{(2)}$  can be approximated quite well by a composite Gaussian function [11]. By straightforward generalization we may obtain similarly the third-order joint histogram  $h^{(3)}(W_A, W_B, W_C)$ .

Now we are ready to connect the histograms with the correlations. Suppose we know the joint probability density function PROB [ $I(x) = A, I(x + d) = B, I(x + 2d) = C$ ], which we call  $p(A, B, C)$ . This joint pdf of the continuous image  $I(x)$  is a close relative of the triple histogram  $h^{(3)}(W_A, W_B, W_C)$ , associated with the binary halftone image  $B(x)$  that simulates the grey-tone image  $I(x)$ . Based on the knowledge of  $p(A, B, C)$  we may compute the third-order correlation as a probabilistic moment

$$\begin{aligned} \langle I^{(3)}(d, 2d) \rangle &= \langle \int I(x) I(x + d) I(x + 2d) dx \rangle \\ &= \int \int \int ABC p(A, B, C) dA dB dC. \end{aligned} \quad (42)$$

In other words, it is possible to obtain the triple correlation in two steps: first, measurement of the joint pdf  $p(A, B, C)$ ; secondly, computation of  $\langle I^{(3)} \rangle$  according to (42). This two-step approach is sensible if  $p(A, B, C)$  is easy to measure, and if the third-moment calculation (42) is simple. In case of halftone pictures, the measurement is easy indeed [10], yielding a result that can be described (in the case of  $p(A, B)$ ) by a composite Gaussian function. Hence, the analytic calculation of the moment is a simple task.

## B. Conditional Motion Probabilities of Micro-Particles or Bacteria

In some biological studies one wants to know the average mobility of a flock of bacteria. To that end we recorded the moving bacteria on a motion picture film. We then measured optically the cross correlation between adjacent frames. The height and the shape of the cross-correlation peak allowed us to make statements about the average motion that took place between two subsequent exposures [12].

Suppose now we wish to know, how many bacteria, that had moved south between exposures at  $t_n$  and  $t_{n+1}$ , decided to move west between  $t_{n+1}$  and  $t_{n+2}$ . In that case, we need three frames  $I_n(\mathbf{x})$ ,  $I_{n+1}(\mathbf{x})$ ,  $I_{n+2}(\mathbf{x})$  to find the answer to our question. We place frame  $I_{n+1}$  upon  $I_n$ , but shifted south by a certain amount. The sandwich  $I_n(\mathbf{x}) \cdot I_{n+1}(\mathbf{x} + \mathbf{s})$  is then correlated with frame  $I_{n+2}(\mathbf{x})$ .

The second-order correlation of the sandwich and frame  $(n+2)$  is a subset of the third-order correlation of all three frames

$$\int I_n(\mathbf{x}) I_{n+1}(\mathbf{x} + \mathbf{s}) I_{n+2}(\mathbf{x} + \mathbf{x}_2) d\mathbf{x} = I_n^{(3)}(\mathbf{x}_1 = \mathbf{s}, \mathbf{x}_2). \quad (43)$$

Fig. 13 shows a model experiment [13], where the bacteria were simulated as holes in an opaque plate. To the left is



Fig. 13. Triple correlation of micro-particles. Left: the sandwich  $I_n(\mathbf{x}) \cdot I_{n+1}(\mathbf{x} + \mathbf{s})$ . Right: the third movie frame  $I_{n+2}(\mathbf{x})$  (from [13]).

the sandwich  $I_n \cdot I_{n+1}$  and to the right the frame  $I_{n+2}$ . The result according to (43) is shown in Fig. 14. The desired triple correlation appears in the first (or minus first) diffrac-



Fig. 14. Result of the triple-correlation experiment (from [13]).

tion order of the optical correlator. Apparently, one quarter of the population of simulated bacteria decided to stay where they were already at  $t_{n+1}$ , the three other quarters moved north, east, and south between  $t_{n+1}$  and  $t_{n+2}$ .

## V. TRIPLE CORRELATION IN ASTRONOMICAL SPECKLE INTERFEROMETRY

Anyone who views an astronomical star with a large telescope will observe a blurred image consisting of a collection of small dots which are wiggling around due to atmospheric turbulence. The typical size of these dots is determined by diffraction on the aperture of the telescope. For an extended object each diffraction dot is expanded to something like a diffraction-limited image of the object. Or in a more mathematical formulation: for frozen turbulence the blurred star image  $I_n(\mathbf{x})$  at time  $t_n$  is described as a convolution (\*) of the astronomical object  $O(\mathbf{x})$  with the combined point-spread function  $P_n(\mathbf{x})$  of the telescope and the turbulent atmosphere

$$I_n(\mathbf{x}) = O(\mathbf{x}) * P_n(\mathbf{x}). \quad (44)$$

It was Labeyrie who realized that in a short exposure the details of the star image are not lost, but merely rearranged or encoded by atmospheric turbulence (Fig. 15) [14].

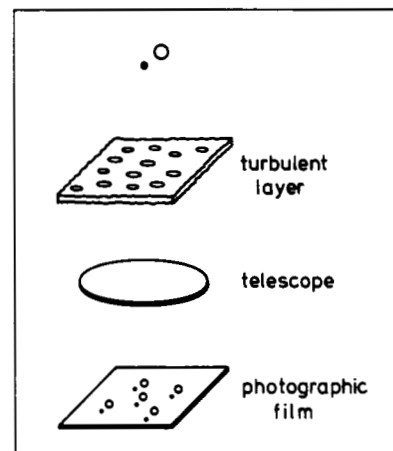


Fig. 15. Formation of a speckle interferogram.

In ordinary astronomical practice the exposure times are several orders of magnitude larger than the time constant of the turbulence ( $\sim 0.1$  s). Hence, the dot structure is wiped out, and with it the encoded information about the fine structure of the astronomical object. As a consequence, the star appears as a big round disc, typically thirty times wider than it should if the turbulent atmosphere were not between the star and the telescope.

### A. Labeyrie's Speckle Interferometry and Speckle Holography

In his speckle-interferometry method Labeyrie evaluated the ensemble averaged autocorrelation of many short exposures, called speckle interferograms [14]. Fig. 16 illustrates that, to a certain extent, the autocorrelation of a speckle interferogram contains a diffraction-limited autocorrelation of the object.

A more rigorous explanation of speckle interferometry can be given in the Fourier domain. Fourier transformation of the raw data  $I_n(\mathbf{u})$  (44) yields

$$\tilde{I}_n(\mathbf{u}) = \tilde{O}(\mathbf{u}) \cdot \tilde{P}_n(\mathbf{u}). \quad (45)$$

Now we average the modulus square of  $\tilde{I}_n(\mathbf{u})$  over many

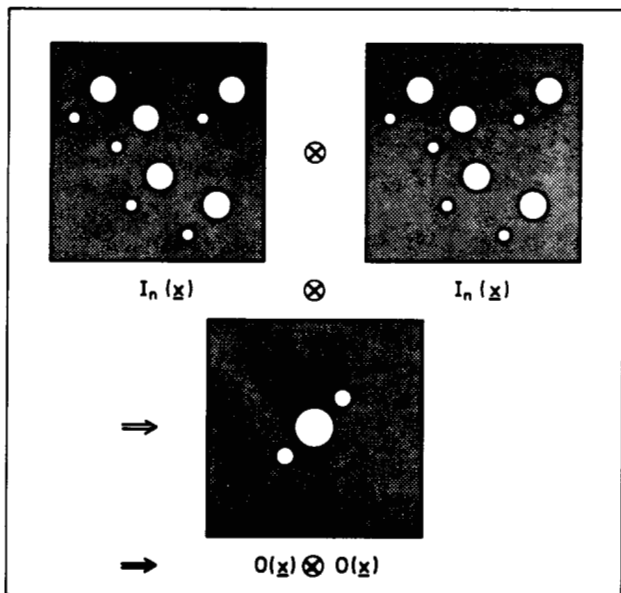


**Fig. 16.** The principle of speckle interferometry: The auto-correlation of speckle interferograms contains in essence the diffraction-limited autocorrelation of the object.

frames of data and obtain

$$\langle |\tilde{I}_n(u)|^2 \rangle = |\tilde{O}(u)|^2 \cdot \langle |\tilde{P}_n(u)|^2 \rangle. \quad (46)$$

The speckle interferometry transfer function  $\langle |\tilde{P}_n(u)|^2 \rangle$  is positive and nonzero for all frequencies  $u$  up to the diffraction limit. Since  $\langle |\tilde{P}_n(u)|^2 \rangle$  is known from theory or by measurement of an isolated star, the object power spectrum  $|\tilde{O}(u)|^2 = \tilde{O}^{(2)}(u)$  can be obtained, providing a diffraction-limited object autocorrelation  $O(x) \otimes O(x) = O^{(2)}(x)$  after Fourier transformation.

Is it possible to unravel true diffraction-limited images instead of autocorrelations as well? A general solution to this problem will be given in the next section. But, first we shall review speckle holography [15] in order to prepare the reader.

In speckle holography, an unresolvable reference star is assumed to be in the neighborhood of the object. In speckle holography the cross correlation of the object speckle interferograms and the corresponding speckle interferograms of the reference are evaluated (Fig. 17). Averaging this process over many frames of data yields, after compensation for the speckle interferometry transfer function, a true image of the object.

In speckle holography, the light from the reference and the object must pass through the same isoplanatic patch of the turbulent atmosphere, in order to form correlated speckle patterns. This condition limits the class of objects which can be studied with the method. But we shall learn that for image reconstruction, the reference star is not necessary at all.

### B. Speckle Masking

In some way speckle masking [16], [17], [4] is a generalization of speckle holography. The new aspect of speckle masking is, that an artificial reference star is produced from the object speckle interferograms by a masking step.

In Fig. 18, the masking step is illustrated for the case of a double star. Multiplication of each speckle interferogram

with the same but properly shifted interferogram yields a speckle pattern which is similar to the pattern of the reference star in speckle holography, at least to a certain extent. The proper shift vector  $s$  is identical to the separation of the double star, which may be known from a speckle interferometry experiment. Finally, we cross correlate ( $\otimes$ ) the artificial reference star with the corresponding object speckle interferogram and average over many frames of

$$\langle [I_n(x) \cdot I_n(x+s)] \otimes I_n(x) \rangle = O(x). \quad (47)$$

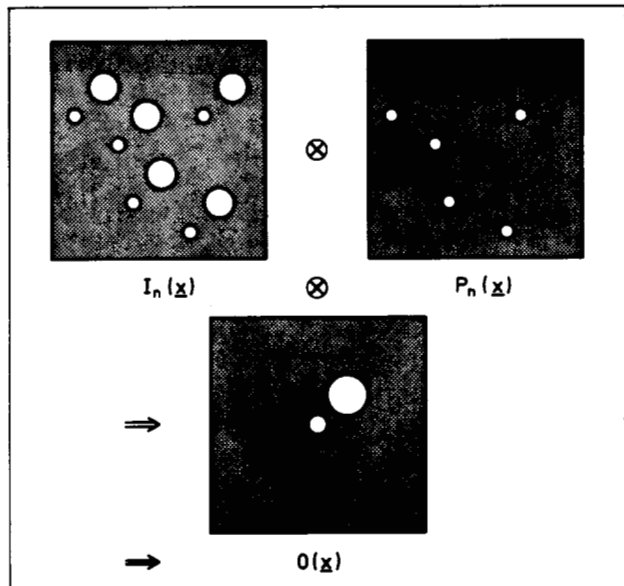


**Fig. 17.** The principle of speckle holography: The cross-correlation of speckle interferograms of the object with the corresponding speckle interferograms of a point source yields a true diffraction-limited image of the object.

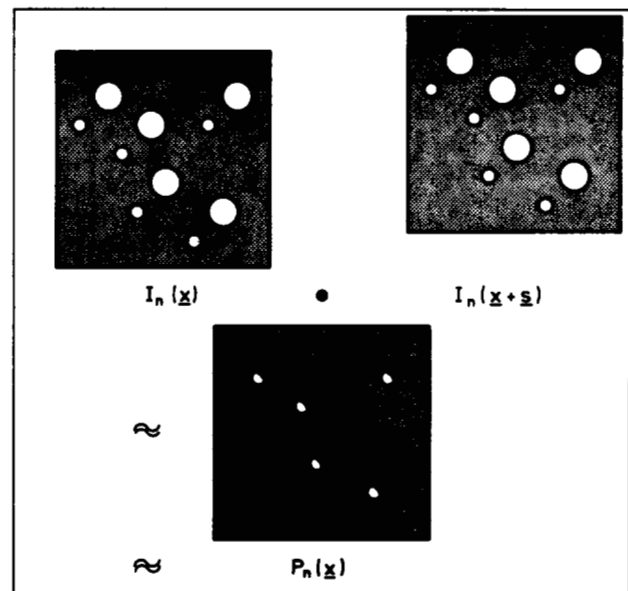


**Fig. 18.** The principle of speckle masking: Multiplication of a speckle interferogram with the same but shifted interferogram forms a mask which can act as an artificial reference star. Cross correlation of the artificial reference mask with the object speckle interferogram yields a true image of the object, similar as in speckle holography (Fig. 16).

The arrow in (47) denotes the compensation of the speckle-masking transfer function, which is not identical to the speckle interferometry transfer function because of systematical errors in the artificial reference star. The result of a speckle-masking experiment is shown in Fig. 19.

Our graphical explanation works well for the image reconstruction of a simple object, like a double star. But, what about complicated general objects?

In order to generalize to arbitrary object we write (47) in our triple notation

$$\begin{aligned} \langle [I_n(\mathbf{x}) \cdot I_n(\mathbf{x} + \mathbf{s})] \otimes I_n(\mathbf{x}) \rangle = \\ \langle \int I_n(\mathbf{x}) \cdot I_n(\mathbf{x} + \mathbf{s}) \cdot I_n(\mathbf{x} + \mathbf{x}_2) d\mathbf{x} \rangle = \\ \langle I_n^{(3)}(\mathbf{x}_1 = \mathbf{s}, \mathbf{x}_2) \rangle. \end{aligned} \quad (48)$$

Now we consider the shift vector  $\mathbf{s}$  as a variable, i.e.,

$$\langle I_n^{(3)}(\mathbf{x}_1, \mathbf{s}) \rangle \rightarrow \langle I_n^{(3)}(\mathbf{x}_1, \mathbf{x}_2) \rangle. \quad (49)$$

Fourier transformation yields

$$\langle \tilde{I}_n^{(3)}(\mathbf{u}_1, \mathbf{u}_2) \rangle = \tilde{O}^{(3)}(\mathbf{u}_1, \mathbf{u}_2) \cdot \langle \tilde{P}_n^{(3)}(\mathbf{u}_1, \mathbf{u}_2) \rangle. \quad (50)$$

Amazingly, the transfer function  $\langle \tilde{P}_n^{(3)}(\mathbf{u}_1, \mathbf{u}_2) \rangle$  in (50) is found to be positive and nonzero for all frequencies up to the diffraction limit. Hence, by dividing by  $\langle \tilde{P}_n^{(3)}(\mathbf{u}_1, \mathbf{u}_2) \rangle$  we obtain the diffraction-limited object bispectrum  $\tilde{O}^{(3)}(\mathbf{u}_1, \mathbf{u}_2)$  [4]. From  $\tilde{O}^{(3)}(\mathbf{u}_1, \mathbf{u}_2)$  true, diffraction-limited images of general astronomical objects can be reconstructed with a high SNR (see Section II-H).

### C. The Influence of Photon Noise

The most interesting astronomical objects are usually very faint and their speckle interferograms consist of only a few isolated photo-events. Such photon-counting speckle interferograms can be described as a sum of delta peaks at the locations  $\mathbf{x}_j$  of the photo-events.

$$D_n(\mathbf{x}) = \sum_{j=1}^N \delta(\mathbf{x} - \mathbf{x}_j) \quad (51)$$

where  $N$  denotes the total number of photons detected in the  $n$ th frame. Both, the number  $N$  and the locations  $\mathbf{x}_j$  vary from frame to frame, of course.

Now we form the ensemble average bispectrum over our photon-counting raw data and find that (see [18])

$$\begin{aligned} \langle \tilde{D}_n^{(3)}(\mathbf{u}_1, \mathbf{u}_2) \rangle = & \bar{N}^3 \langle \tilde{i}_n^{(3)}(\mathbf{u}_1, \mathbf{u}_2) \rangle \\ & + \bar{N}^2 \langle \tilde{i}_n^{(2)}(\mathbf{u}_1) + \tilde{i}_n^{(2)}(\mathbf{u}_2) \\ & + \tilde{i}_n^{(2)}(-\mathbf{u}_1 - \mathbf{u}_2) \rangle + \bar{N} \end{aligned} \quad (52)$$

where the lower case letters denote normalized spectra and bispectra ( $\tilde{i}(0) = \tilde{i}^{(3)}(0,0) = 1$ ) and where  $\bar{N}$  denotes the average number of photons per speckle interferogram.

For image reconstruction we need to ensemble average bispectrum  $\langle \tilde{i}_n^{(3)}(\mathbf{u}_1, \mathbf{u}_2) \rangle$  of the classical intensity falling onto the detector. From (54) we see that  $\langle \tilde{i}_n^{(3)}(\mathbf{u}_1, \mathbf{u}_2) \rangle$  can be derived from  $\langle \tilde{D}_n(\mathbf{u}_1, \mathbf{u}_2) \rangle$  after compensation of the photon bias which contains second-order correlations. These second-order correlations can be found by evaluating the ensemble average power spectrum of the raw data

$$\langle |\tilde{D}_n(\mathbf{u}_1)|^2 \rangle = \bar{N} + \bar{N}^2 \langle |\tilde{i}_n(\mathbf{u}_1)|^2 \rangle. \quad (53)$$

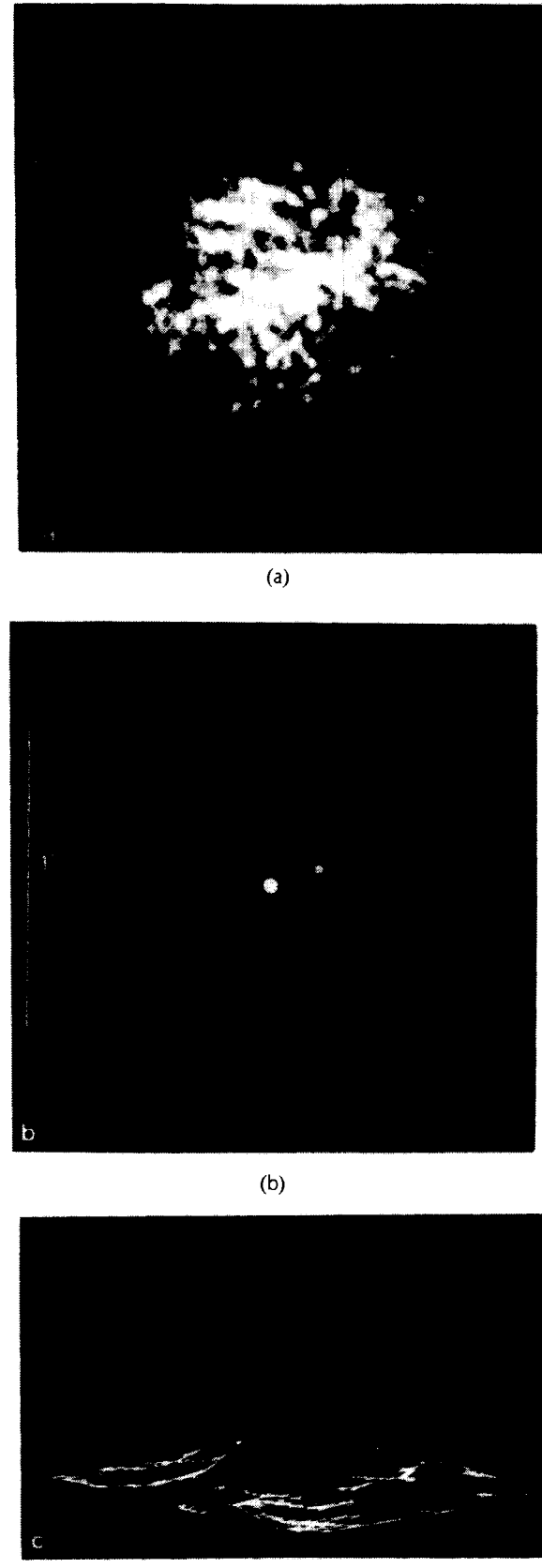


**Fig. 19.** A speckle-masking experiment based on 300 speckle interferograms of the double star Psi-Scuti. (a) A typical speckle interferogram. (b), (c) The reconstructed true image. (Epoch: 1982.378, separation:  $0.184'' \pm 0.004''$ ) (from [17]).

Astronomers are interested especially in very faint objects. Hence, we ask the question: how many photons per frame do we have to observe in order to obtain a decent SNR?

In order to answer this question, a comparison with speckle interferometry seems sensible, assuming the same set of raw data. Speckle interferometry has already been applied to objects of 17th magnitude. A theoretical estimation of the SNR showed [18] that image reconstruction from bispectra is superior to the power spectrum analysis in speckle interferometry if the average number of photons per speckle interferogram exceeds four. This superiority is due to the fact that the bispectrum contains highly redundant signal information. Or in other words, cubic averaging is less destructive than quadratic averaging, as performed in ordinary speckle interferometry.

## VI. OTHER PROJECTS WITH TRIPLE CORRELATIONS

### A. Methods

In this subsection we will briefly mention methods for implementing triple correlations. Applications thereof will follow in subsection VI-B.

The majority of the proposed methods rely on acoustooptics. For a cross triple correlation one signal  $I_s(t)$  may modulate a light source. The light falls upon a moving acoustooptical wave  $I_y(t + y/c)$  and thereafter on another acoustical wave  $I_x(t + x/c)$ , moving in an orthogonal direction (see Fig. 20). A two-dimensional time-integrating receiver will record the triple correlation

$$I_{syx}^{(3)}(y, x) = \int I_s(t) I_y(t + y/c) I_x(t + x/c) dt. \quad (54)$$

For real-time applications, a spatially integrating method will be appropriate. One of the signals may be a fixed mask  $I_m(x)$ . The second signal may move upwards  $I_u(x - y + c_u t)$ , the third one downwards, like  $I_d(x + y + c_d t)$ . The two velocities may be arranged to differ due to different angles of inclination or due to an optical magnification on the way from  $I_u$  to  $I_d$ . The optical system is set up such that integration takes place only in the x-direction, with the following outcome:

$$\begin{aligned} & I_{mud}^{(3)}(-y + c_u t, +y + c_d t) \\ &= \int I_m(x) I_u(x - y + c_u t) I_d(x + y + c_d t) dx. \end{aligned} \quad (55)$$

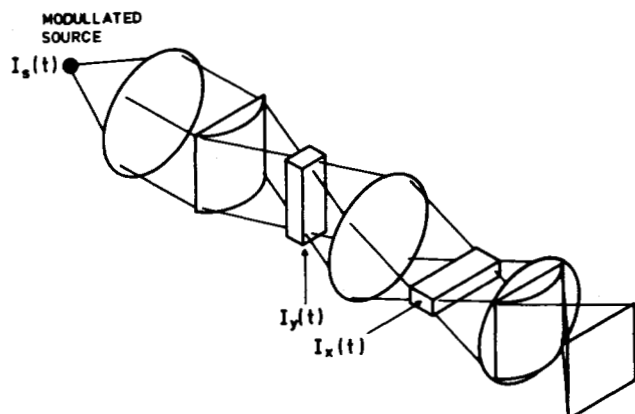


Fig. 20. An acoustooptic triple correlator.

These are merely two typical examples out of a family of AO correlators [19]–[21].

Other methods can be found by looking for triple-product integrals in textbooks on theoretical optics. One example of that approach is a triple correlator based on the theory of partial coherence. The source distribution and two shifted versions of the pupil function appear in a formula that determines the fringe modulation of a grating image [22].

Yet another approach for finding new triple-correlation methods is to look for signal processing systems with three entrance ports. The RUBIC cubic processor is such a system [23].

### B. Some Applications

For these authors the significance of the triple correlation became apparent when reading some papers by T. Sato and co-workers [24]–[26]. One of their application examples rests on the fact that the triple correlation of a pure sinusoid is zero. But as soon as a small amount of higher harmonic oscillations is added the triple correlation will emerge. If proper functioning of a mechanical system results in a pure sinusoid tone, and if beginning mechanical deteriorations cause higher harmonics to be generated, a triple-correlation detector will be a sensitive control unit. The same basic concept has been used by others for studying the propagation of ocean waves in shallow water with uneven ocean floor [27].

Gamo [7] realized a shortcoming of Hanbury Brown's intensity interferometer, which yields only the power spectrum of the source configuration. That method detects second-order intensity correlations, which may be interpreted also as fourth-order amplitude correlation. Gamo suggested measuring third-order intensity correlations. The theory, which is sketched at the end of our Section II shows that the third-order intensity correlations yield more information than second-order intensity correlations do.

Gamo also realized, that the intensity triple correlation of fluctuating photocurrents may be used to analyze spectrum profiles of light beams [6]. Meanwhile, third-order photon-correlation techniques have been applied to study properties of laser light [28].

In a holographic associative memory, a pair of messages (or pictures) is stored jointly. When addressing that memory with a third message, the response is an integral expression with all three messages as a triple product under an integral [22]. In that sense, an associative holographic memory can be considered as a triple correlator. A similar experiment can be performed in real time with the help of a third-order nonlinear optical material, such as that used in four-wave mixing, especially in phase conjunction. Also the ambiguity function and the Wigner distribution function are special cases of a triple correlation. Triple correlations were also considered by Goodman [29] in a recent study on architectures of optical data processing systems.

## VII. CONCLUSIONS

The second-order correlation plays a significant role in signal processing. Not so the third-order correlation. Partially, this may be so because of a feeling that the third-order correlation has no more to offer than the second-order correlation. We hope we have been able to dispell that unjustified feeling, because the third-order correlation is fundamentally superior in some aspects.

## ACKNOWLEDGMENT

Many fruitful discussions with our colleagues H. E. Reinfelder, G. Stucke, Ch. Thum, J. Uebler, and G. P. Weigelt are gratefully acknowledged. In addition, one of the authors (AWL) wishes to express his appreciation to T. Sato for a stimulating discussion.

## REFERENCES

- [1] D. R. Brillinger, *Time Series Analysis*. New York: Holt, Rinehardt and Winston, 1975.
- [2] A. W. Lohmann, "The holographic principle," in *NATO Workshop on Inverse Scattering*, W. M. Boerner, Ed. Chicago, IL: Windshiem 1983.
- [3] A. Grünbaum, private communication, Dept. of Math., Univ. of California, Berkeley, CA, USA.
- [4] A. W. Lohmann, G. P. Weigelt, and B. Wirnitzer, "Speckle masking in astronomy—Triple correlation theory and applications," *Appl. Opt.*, vol. 22, no. 24, Dec. 1983.
- [5] H. O. Bartelt, A. W. Lohmann, and B. Wirnitzer, "Amplitude and phase recovery from bispectra," *J. Opt. Soc. Amer.* (submitted).
- [6] H. Gamo, "Triple correlator of photo electric fluctuations as a spectroscopic tool," *J. Appl. Phys.*, vol. 34, no. 4, pp. 875–876, Apr. 1963.
- [7] ———, "Phase determination of coherence functions by the intensity interferometer," in *Symposium on Electromagnetic Theory and Antennas*. New York: Pergamon, 1963, pp. 801–810.
- [8] C. V. Shank, "Measurement of ultrafast phenomena in the femtosecond time domain," *Science*, vol. 219, pp. 1027–1031, Mar. 1983.
- [9] B. Wirnitzer, "Measurement of ultrashort laser pulses," *Opt. Commun.*, vol. 48, no. 3, pp. 225–228, Dec. 1983.
- [10] A. W. Lohmann and Ch. Thum, "Measurement of histograms of halftone images," *Opt. Commun.*, vol. 31, no. 2, pp. 114–118, Nov. 1979.
- [11] Ch. Thum, "Hybrid measurements of image histograms, with an application to texture discrimination," *Opt. Acta*, vol. 30, no. 11, pp. 1665–1673, Nov. 1983.  
———, "Measurement of the entropy of an image with application to image focusing," *Opt. Acta* (accepted).
- [12] H. Böhm, A. W. Lohmann, and G. P. Weigelt, "Method for measuring the average motion of a large number of biological objects," *Opt. Lett.*, vol. 6, no. 4, pp. 162–164, Apr. 1981.
- [13] A. W. Lohmann, J. Uebler, and G. P. Weigelt, "Conditional motion probabilities of micro-particles," *Opt. Commun.*, vol. 49, no. 4, pp. 238–240, Mar. 1984.
- [14] A. Labeyrie, "Attainment of diffraction-limited resolution in large telescopes by Fourier analysing speckle patterns in star images," *Astron. Astrophys.*, vol. 6, p. 85, 1970.  
———, "High resolution techniques in optical astronomy," in *Progress in Optics*, vol. XIV, E. Wolf, Ed. Amsterdam, The Netherlands: North-Holland, 1976, pp. 46–87.
- [15] C. Y. C. Liu and A. W. Lohmann, "High resolution image formation through the turbulent atmosphere," *Opt. Commun.*, vol. 8, no. 4, pp. 372–377, 1973.  
R. H. T. Bates, P. T. Gough, and P. J. Napier, "Speckle holography," *Astron. Astrophys.*, vol. 22, p. 314, 1973.  
P. T. Gough and R. H. T. Bates, "Speckle holography," *Opt. Acta*, vol. 21, no. 3, pp. 243–254, Mar. 1974.
- [16] G. P. Weigelt, "Speckle holography measurements of the stars Zeta Cancri and ADS 3358," *Appl. Opt.*, vol. 17, no. 17, pp. 2660–2662, Sept. 1978.
- [17] G. P. Weigelt, "Modified speckle interferometry: Speckle masking," *Opt. Commun.*, vol. 21, no. 1, pp. 55–59, Apr. 1977.
- [18] B. Wirnitzer, "Bispectral analysis at low light levels and speckle masking," *J. Opt. Soc. Amer.* (submitted).
- [19] P. Kellman, "Time integrating optical processors," in *Optical Processing Systems (Proc. SPIE)*, vol. 185, 1979, pp. 130–139, 1979.  
———, "Time integrating optical signal processing," *Opt. Eng.*, vol. 19, no. 3, pp. 370–375, May/June 1980.
- [20] T. M. Turpin, "Spectrum analysis using optical processing," *Proc. IEEE*, vol. 69, no. 1, pp. 79–92, Jan. 1981.  
W. T. Rhodes, "Acousto-optic signal processing: Convolution and correlation," *Proc. IEEE*, vol. 69, no. 1, pp. 65–79, Jan. 1981.  
D. Casasent and G. Silberschatz, "Product code processing on a triple product processor," *Appl. Opt.*, vol. 21, no. 11, pp. 2076–2084, June 1982.  
J. M. Florence and J. H. Song, "Real-time acousto-optic bispectral processor," *SPIE Proc.*, vol. 431, paper no. 431-36, 1983.  
C. Lin, "Compact acousto-optical signal processor for real-time Fourier transformation," *Appl. Opt.*, vol. 21, no. 18, pp. 327–328, Sept. 1983.
- [21] M. J. Berg and J. N. Lee, "Acousto-optic signal processing theory and implementations," in *Optical Engineering*, vol. 2. New York: Marcel Dekker, 1983.
- [22] A. W. Lohmann, "Chances for optical computing," *Optik*, vol. 65, no. 1, pp. 9–16, 1983.
- [23] R. P. Bocker, "Advanced RUBIC cube processor," *Appl. Opt.*, vol. 22, no. 16, pp. 2401–2402, Aug. 1983.
- [24] K. Sasaki, T. Sato, and Y. Nakamura, "Holographic passive sonar," *IEEE Trans. Sonics Ultrason.*, vol. SU-24, no. 3, pp. 193–200, May 1977.  
T. Sato, S. Wadaka, J. Yamamoto, and J. Ishii, "Imaging system using an intensity triple correlator," *Appl. Opt.*, vol. 17, no. 13, pp. 2047–2052, July 1978.  
T. Sato, S. Wadaka, and J. Ishii, "A new ultrasonic imaging system by using rotating random phase disk and power spectral and third order correlation analysis," in *7th Intern. Symp. on Acoustic Imaging and Holography Proc.*, vol. 16, 1976.  
T. Sato and K. Sasaki, "Bispectral holography," *J. Acoust. Soc. Amer.*, vol. 62, no. 2, p. 404, 1977.
- [25] T. Sato and O. Sasaki, "New 3-D laser Doppler velocimeter using cross-bispectral analysis," *Appl. Opt.*, vol. 17, no. 24, pp. 3890–3894, Dec. 1978.  
O. Sasaki, T. Sato, and T. Oda, "Laser Doppler vibration measuring system using bispectral analysis," *Appl. Opt.*, vol. 19, no. 1, pp. 151–153, Jan. 1980.
- [26] T. Sato, K. Sasaki, and Y. Nakamura, "Real-time bispectral analysis of gear noise and its application to contactless diagnosis," *J. Acoust. Soc. Amer.*, vol. 62, no. 2, p. 404, 1977.  
———, "Real-time bispectral analysis of gear noise and its application to contactless diagnosis," *Bull. R.L.P.M. of Tokyo Inst. Technol.*, vol. 38, p. 9, 1976.
- [27] K. Hasselmann, M. Munk, and G. McDonald, "Bispectra of ocean waves," in *Proc. Symp. on Time Series Analysis*, M. Rosenblatt, Ed., pp. 125–139, 1962.
- [28] S. Chopra and L. Mandel, "Higher-order correlation properties of a laser beam," *Phys. Rev. Lett.*, vol. 30, no. 2, pp. 60–63, 1972.  
M. Corti and V. Degiorgio, "Third-order intensity correlations in laser light," *Opt. Commun.*, vol. 11, no. 1, pp. 1–4, May 1974.
- [29] J. Blake and R. Barakat, "Three-fold photoelectron-counting statistics for Gaussian light," *Opt. Commun.*, vol. 16, no. 3, pp. 303–306, Mar. 1976.
- [30] J. W. Goodman, "Architectural development of optical data processing systems," *I.E.E.E. (Austr.)*, vol. 2, pp. 139–149, 1982.  
D. Brillinger and M. Rosenblatt, in *Spectral Analysis of Time Series*, B. Harris, Ed. New York: Wiley, 1967.  
T. Sato, *Lecture Notes at the National Bureau of Standards*, Washington, DC, 1978.

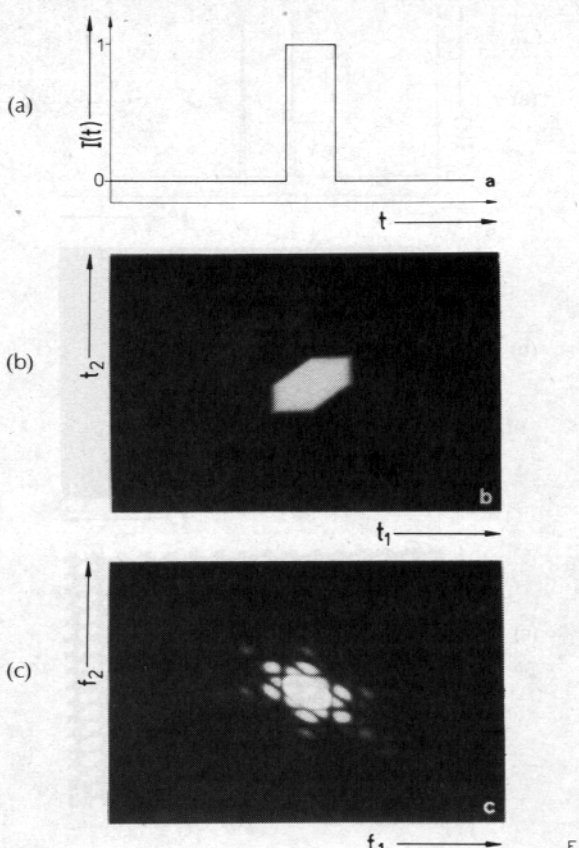


**Fig. 1.** Triple correlation (b) and bispectrum (c) for a square-box signal (a).

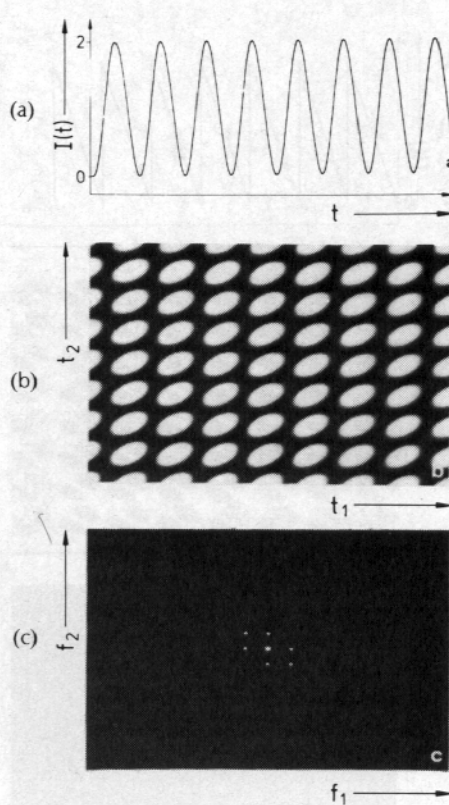


**Fig. 2.** Triple correlation (b) and bispectrum (c) for a cosine signal on a bias (a).

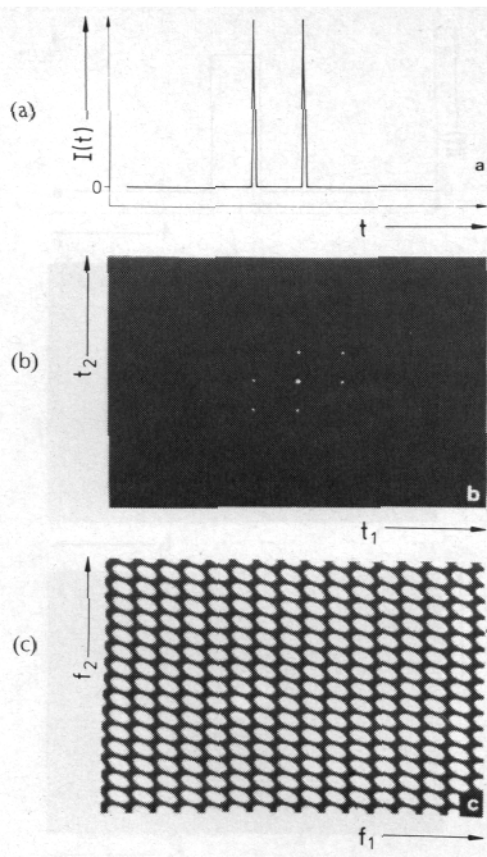


**Fig. 3.** Triple correlation (b) and bispectrum (c) for a signal, consisting of two spikes (a).

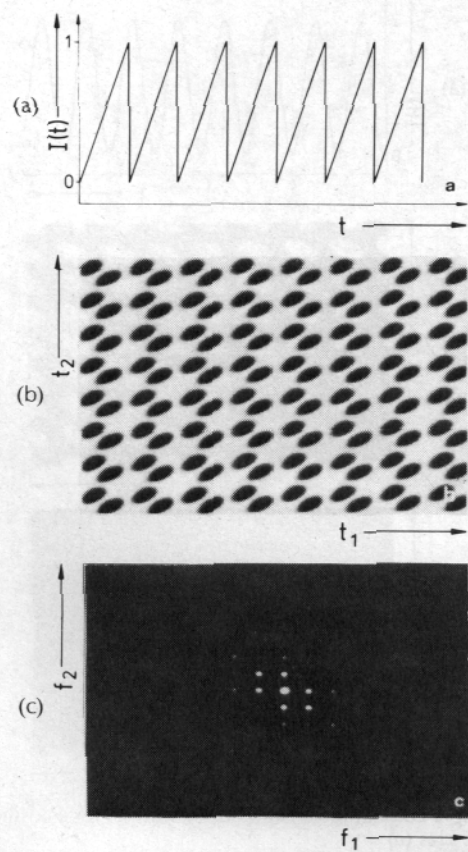


**Fig. 4.** Triple correlation (b) and bispectrum (c) for a sawtooth-periodical signal (a).

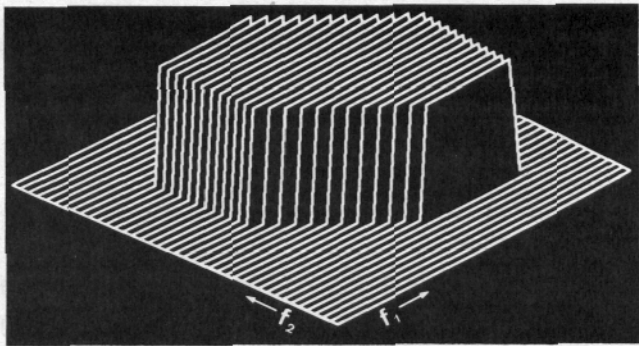


**Fig. 5.** The bispectral low pass, associated with the square-box low-pass filter function.

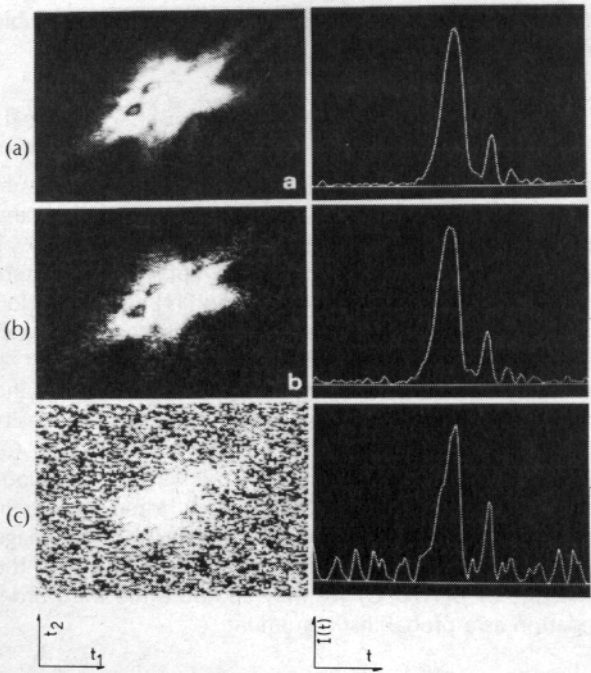
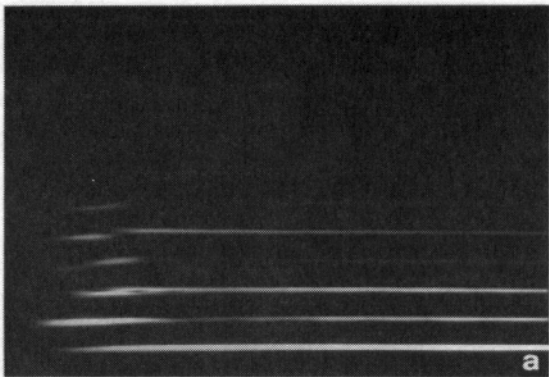
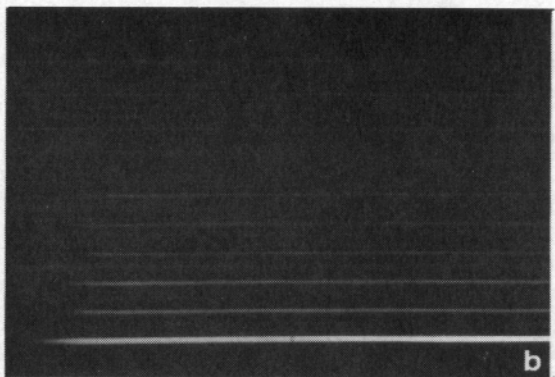


**Fig. 9.** Signal reconstruction from triple correlations. From the intensity triple correlation of the pulse shape (left column), the true pulse shape can be reconstructed (right column). The SNR in the triple correlation was (a) 4, (b) 2, (c) 0.4. The higher SNR of the reconstructed pulse shapes is due to redundant signal information which is contained in the triple correlation (for further details see [9]).

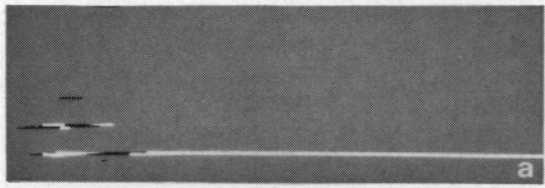


(a)

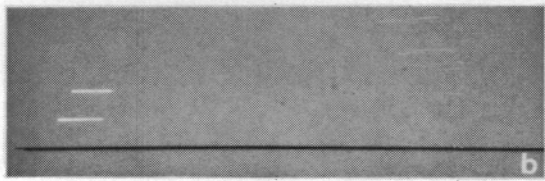


(b)

**Fig. 10.** Musical timbre, presented as a spectrogram. Tone "a" of a flute of good quality (a) and of a flute of poor quality (b).



(a)



(b)

**Fig. 11.** Phase of the complex bispectrogram. Tone "a" of a flute of good quality (a) and of a flute of poor quality (b). The phase values ( $-\pi$  to  $+\pi$ ) are displayed as intensities.

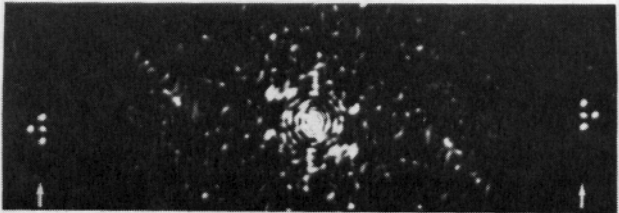
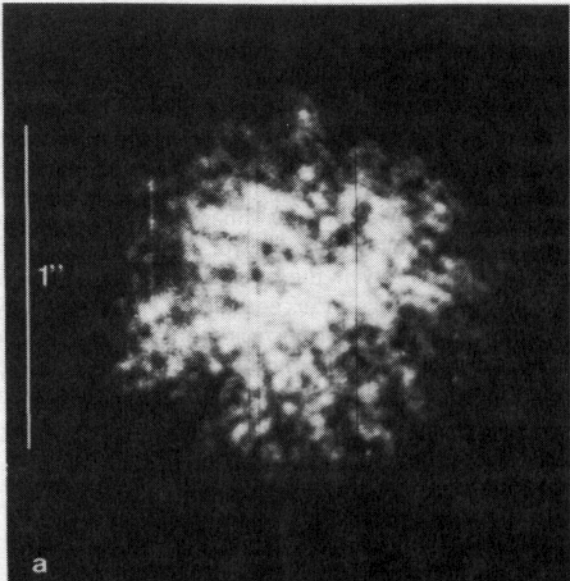
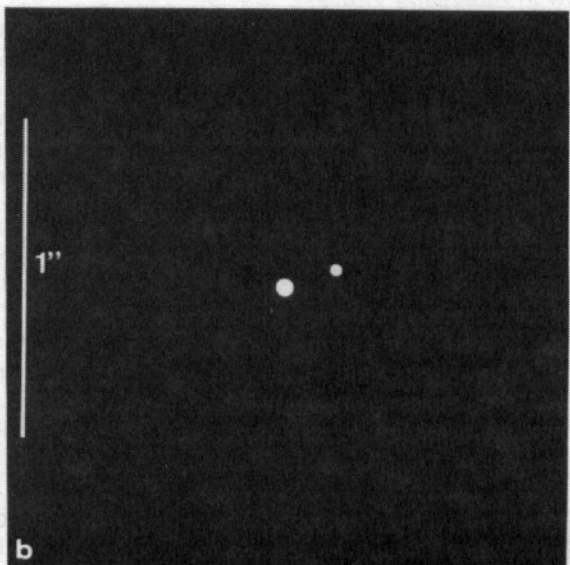


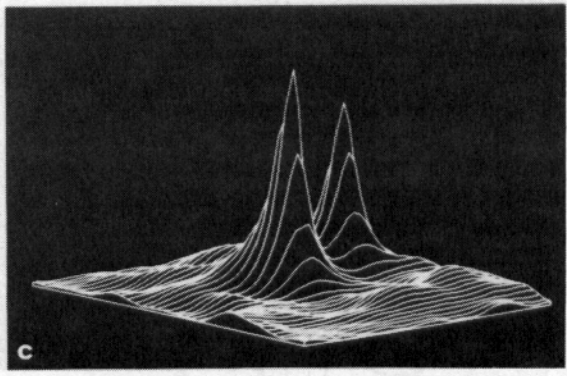
**Fig. 14.** Result of the triple-correlation experiment (from [13]).



(a)



(b)



(c)

**Fig. 19.** A speckle-masking experiment based on 300 speckle interferograms of the double star Psi-SGR. (a) A typical speckle interferogram. (b), (c) The reconstructed true image. (Epoch: 1982.378, separation:  $0.184'' \pm 0.004''$ ) (from [17]).